Advances in Engineering Software 100 (2016) 266–276

Contents lists available at ScienceDirect

Advances in Engineering Software

journal homepage: www.elsevier.com/locate/advengsoft

Trajectory optimization for lunar soft landing with a Hamiltonian-based adaptive mesh refinement strategy

Lin Ma[a,1], Zhijiang Shao[a,2,*], Weifeng Chen[b,3], Zhengyu Song[c,4,*]

[a] Zhejiang University, Hangzhou, China, 310027
[b] Zhejiang University of Technology, Hangzhou, China, 310023
[c] National Key Laboratory of Science and Technology on Aerospace Intelligent Control, Beijing, China, 100854

ARTICLE INFO

Article history:
Received 20 April 2016
Revised 30 June 2016
Accepted 1 August 2016
Available online 9 August 2016

Keywords:
Trajectory optimization
Lunar soft landing
Simultaneous dynamic optimization approach
Adaptive mesh refinement
R-function method
Computational guidance and control

ABSTRACT

In this study, the problem of fuel-optimal lunar soft landing trajectory optimization using variable-thrust propulsion is considered. First, the lunar soft landing trajectory optimization problem with three-dimensional kinematics and dynamics model, boundary conditions, and path constraints strictly described is formulated. Then, the formulated trajectory optimization problem is solved by the simultaneous dynamic optimization approach. With bounds imposed on the magnitude of engine thrust, the optimal control solutions typically have a "bang-bang" thrust profile. The general simultaneous dynamic optimization approach has difficulty handling breakpoints in the control profiles. A novel adaptive mesh refinement strategy based on a constant Hamiltonian profile is proposed to address the difficulty of locating breakpoints in the thrust profile. Two cases are simulated. The engine of the first case is throttleable between zero and full thrust. The engine of the second case is throttleable between 10% and 60% of full thrust, and at full thrust. Union property of *R*-function method is utilized to express the thrust profile of the second case in the trajectory optimization problem. Simulation results show that the enhanced simultaneous dynamic optimization approach with adaptive mesh refinement strategy can effectively capture the breakpoints in the optimal thrust profile and obtain more refined lunar soft landing optimal solutions, compared with the results obtained by the general simultaneous dynamic optimization approach.

1. Introduction

Recently, exploration of the moon, the nearest celestial body to the earth, has become increasingly attractive for space scientists for several reasons. For example, Helium-3, which is used in nuclear fusion and could be a future energy source, is abundant on the Moon. The existence of water has also been confirmed by the National Aeronautics and Space Administration's (NASA) Lunar Crater Observation and Sensing Satellite. Furthermore, the Moon can be an advance base for exploring other planets [1,2]. Given the potential benefits of lunar exploration, Americans, Europeans, Japanese, Chinese, and Indians are all planning to go back to the Moon [3]. After conducting the Apollo Program from 1961 to 1972, NASA officials have not started any new lunar programs. However, this development does not mean that scientists and engineers at NASA have lost interest in the moon. NASA has recently launched Lunar CATALYST, a program designed to assist and encourage private companies that are interested in lunar exploration [4].

In lunar exploration, lunar soft landing is a challenging problem, in which the lunar module (LM) lands softly on the moon surface using the reverse force of the propeller. This study aims to obtain the fuel-optimal trajectory of lunar soft landing with variable thrust. This lunar soft landing trajectory optimization problem is formulated as a constrained optimal control problem incorporated with the main specific features of the problem.

Current studies on the lunar soft landing optimal control problem are mainly based on optimal control theory. Ref. [5] applied Pontryagin maximum principle to develop a fuel-optimal thrust program for the terminal phase of a lunar soft-landing mission. Ref. [6] optimized the perilune altitude of the intermediate orbit for lunar landing trajectory in addition to the optimal thrust program. Ref. [7] applied a variable-time-domain neighboring optimal guidance algorithm, which is capable of driving a dynamical system along the specified nominal and optimal paths, to lunar

* Corresponding authors.
E-mail addresses: lma@zju.edu.cn (L. Ma), szj@zju.edu.cn (Z. Shao), wfchen@zjut.edu.cn (W. Chen), zycalt12@sina.com (Z. Song).

[1] Ph. D. Candidate, College of Control Science and Engineering, and Member AIAA.
[2] Full Professor, College of Control Science and Engineering, State Key Laboratory of Industrial Control Technology.
[3] Associate Professor, Department of Automation, College of Information Engineering
[4] Vice Chief Designer, National Key Laboratory of Science and Technology on Aerospace Intelligent Control.

http://dx.doi.org/10.1016/j.advengsoft.2016.08.002
0965-9978/

descent and soft landing. Ref. [8] constructed a fuel-optimal guidance law to ensure the soft landing of the LM with the terminal attitude of the module within a small deviation from being vertical with respect to the lunar surface, which is solved by applying the control parameterization technique and a time scaling transform. Ref. [9] outlined a design for a targeting algorithm that quickly and reliably generates a two-dimensional reference trajectory and a real-time three-dimensional guidance algorithm that can use this or any reference trajectory as its basis. Ref. [10] developed a computational method based on control parameterization in conjunction with a time scaling transform and the constraint transcription method to design the optimal controller for the constrained lunar descent optimal control problem. Refs. [1] and [2] conducted the two-dimensional and three-dimensional multiphase trajectory optimization for soft lunar landing from a parking orbit with the pseudospectral method, respectively.

Numerical methods for the optimal control problem fall into two general categories, namely, indirect methods and direct methods [11]. Indirect methods have several disadvantages, including a small region of convergence, the need to derive the Hamiltonian boundary value problem analytically, a non-intuitive initial guess for the costate, and a priori knowledge of the constrained and unconstrained arcs if path constraints are present [12]. Moreover, most optimal control problems do not have an analytical solution. The key of optimal control strategies is the need to determine optimal trajectories for complex system models with efficient and reliable nonlinear programming (NLP) methods [13], which illustrates that direct methods are preferable to solve complex optimal control problems. Pseudospectral methods [12,14–20], which are a class of direct methods where the optimal control problem is transcribed into an NLP problem, have recently become increasingly popular and widely used to obtain the numerical solution of optimal control problems. The state and control variables are parameterized using global polynomials at collocation nodes derived from a Gaussian quadrature. For problems whose solutions are smooth, the application of global polynomials associated with Gaussian quadrature collocation points provides accurate approximations and exponential convergence [20]. Collocation points are commonly divided into three sets, namely, Legendre-Gauss, Legendre-Gauss-Radau, and Legendre-Gauss-Lobatto points. However, for problems whose solutions are nonsmooth or not well approximated by global polynomials, a simultaneous dynamic optimization approach [18,21,22] is preferable. In the simultaneous dynamic optimization approach, the time interval is partitioned into subintervals, and the differential-algebraic equations (DAEs) are discretized to algebraic equations over each subinterval called finite element.

The thrust of the LM is throttleable and bounded in this study. For the fuel-optimal lunar descent problem with bounded magnitude of thrust, the optimal thrust profile typically has a "bang-bang" profile: the thrust magnitude "bangs" instantaneously between its maximum and minimum magnitudes [23]. Thus, breakpoints exist in the thrust profile. Direct methods are challenged by the need to capture discontinuities (breakpoints) in control profiles accurately [13]. This study proposes a novel adaptive mesh refinement strategy based on a constant Hamiltonian profile to enhance the general simultaneous dynamic optimization approach to address the difficulty of locating breakpoints in the thrust profile in this trajectory optimization problem.

The remainder of this paper is organized as follows: Section 2 establishes the lunar soft landing trajectory optimization problem. Section 3 introduces the simultaneous dynamic optimization approach. Section 4 presents the proposed adaptive mesh refinement strategy. Section 5 presents the numerical results and discussions. Section 6 gives the conclusion.

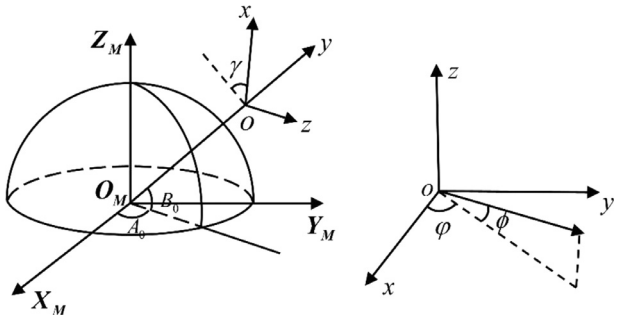

Fig. 1. Coordinates of lunar soft landing.

2. Lunar soft landing trajectory optimization problem

The kinematics and dynamics model of the lunar soft landing process, where LM is modeled as a mass point, is described with the assumption that the moon is a regular spherical body and the influences of the moon's rotation and other celestial bodies on LM are neglected.

2.1. Kinematics and dynamics model

The lunar soft landing process can be treated in a two-body system. The motion of lunar soft landing is described in three-dimensional coordinates in Fig. 1. This study assumes that $O_MX_MY_MZ_M$ and $oxyz$ are the Lunar Central Inertial Coordinate and the Lunar Descent Inertial Coordinate, respectively. The kinematics and dynamics equations of the lunar descent process in the Lunar Descent Inertial Coordinate are expressed as follows:

$$\begin{aligned}
&\frac{dx}{dt} = V_x, \quad \frac{dy}{dt} = V_y, \quad \frac{dz}{dt} = V_z \\
&\frac{dV_x}{dt} = \frac{T}{m}\cos\varphi\cos\phi - \frac{\mu x}{(x^2+y^2+z^2)^{3/2}} \\
&\frac{dV_y}{dt} = \frac{T}{m}\sin\varphi\cos\phi - \frac{\mu y}{(x^2+y^2+z^2)^{3/2}} \\
&\frac{dV_z}{dt} = -\frac{T}{m}\sin\phi - \frac{\mu z}{(x^2+y^2+z^2)^{3/2}} \\
&\frac{dm}{dt} = -\frac{T}{I_{sp}g_0}
\end{aligned} \tag{1}$$

where (x, y, z) is the position vector of LM; (V_x, V_y, V_z) is the velocity vector of LM; m is the mass of LM; φ and ϕ represent the pitch and yaw angles, respectively; T denotes the thrust magnitude; I_{sp} is the specific impulse; and μ and g_0 denote the moon's gravitational constant and the Earth's gravitational acceleration, respectively. The positive directions of ox-axis, oy-axis, and oz-axis are named tangential direction, radial direction, and lateral direction, respectively.

2.2. Path constraints

The thrust is throttleable in full range from the lower value to the upper value in this study, thus the constraint for thrust is expressed as follows:

$$0 \le T \le T_{\max} \tag{2}$$

where $T_{\max}$ is the maximum thrust value. To avoid sudden angle changes during flight, the following constraints are applied to satisfy the angular rate of the pitch and yaw angles:

$$|d\varphi/dt| \le \omega_{\alpha\max}, \ |d\phi/dt| \le \omega_{\beta\max} \tag{3}$$

where $\omega_{\alpha\,\max}$ and $\omega_{\beta\,\max}$ are the maximum angular rates of the pitch and yaw angles, respectively. Given that the flight is over the surface of the moon, the following expression can be derived:

$$\sqrt{x^2+y^2+z^2} \geq R_M \tag{4}$$

where R_M is the radius of the moon.

2.3. Boundary constraints

The initial constraints are expressed as follows:

$$\begin{aligned} &x(0)=x_0, y(0)=y_0, z(0)=z_0, m(0)=m_0\\ &V_x(0)=V_{x0}, V_y(0)=V_{y0}, V_z(0)=V_{z0} \end{aligned} \tag{5}$$

The LM lands at a specified point, thus the terminal position and velocity constraints are expressed as follows:

$$\begin{aligned} &x(t_f)=x_f, y(t_f)=y_f, z(t_f)=z_f\\ &V_x(t_f)=0, V_y(t_f)=0, V_z(t_f)=0 \end{aligned} \tag{6}$$

In this study, the initial position and landing position of the LM are given as (A_0, B_0, H_0) and (A_f, B_f, H_f), where (A_0, B_0, H_0) refers to the longitude, latitude, and height of the LM's initial position, and (A_f, B_f, H_f) denotes the longitude, latitude, and height of the LM's landing. In Fig. 1, γ is the angle between the ox-axis and the north direction. The initial position and landing position of the LM in the Lunar Central Inertial Coordinate are expressed as follows:

$$\begin{cases} x_{M0}=H_0\cos B_0\cos A_0\\ y_{M0}=H_0\cos B_0\sin A_0\\ z_{M0}=H_0\sin B_0 \end{cases} \quad \begin{cases} x_{Mf}=H_f\cos B_f\cos A_f\\ y_{Mf}=H_f\cos B_f\sin A_f\\ z_{Mf}=H_f\sin B_f \end{cases} \tag{7}$$

The coordinate $oxyz$ is deduced from the coordinate $O_MX_MY_MZ_M$ by a rotation $-(\pi/2-A_0)$ around the Z_M-axis, then followed a rotation B_0 around the X_M-axis, finally followed a rotation $-(\pi/2+\gamma)$ around the Y_M-axis. Therefore, the transformation matrix equation is written as follows:

$$T_1 = L_{YM}(-(\pi/2+\gamma))L_{XM}(B_0)L_{ZM}(-(\pi/2-A_0)) \tag{8}$$

where L_{XM}, L_{YM}, and L_{ZM} are defined as the elementary matrices to describe rotation around the X_M-axis, Y_M-axis, and Z_M-axis, respectively. Thus, the following expression can be derived:

$$\begin{aligned} &(x_0,y_0,z_0)^T = T_1(x_{M0},y_{M0},z_{M0})^T\\ &(x_f,y_f,z_f)^T = T_1(x_{Mf},y_{Mf},z_{Mf})^T \end{aligned} \tag{9}$$

2.4. Objective function

The objective of this lunar soft landing trajectory optimization problem is to minimize the fuel consumption when LM lands at the specified point, i.e.,

$$J=-m(t_f) \tag{10}$$

Then, the lunar soft landing trajectory optimization problem is described as follows:

The objective function given in Eq. (10) is minimized subject to the dynamics constraints of Eq. (1), the path constraints given in Eqs. (2)–(4), and the boundary constraints given in Eqs. (5) and (6).

3. Simultaneous dynamic optimization approach

Without loss of generality, the following general dynamic optimization problem is considered [21,22]:

$$\begin{aligned} &\min\ \Phi(z(t_f))\\ &s.t.\quad \frac{dz}{dt}=f(z(t),y(t),u(t)),\ z(t_0)=z_0\\ &\qquad g(z(t),y(t),u(t))=0\\ &\qquad u_L\leq u(t)\leq u_U\\ &\qquad \psi(z(t_f))\leq 0 \end{aligned} \tag{11}$$

where $z(t)$ and $y(t)$ are the differential and algebraic state profiles, respectively, and $u(t)$ denotes the control profiles. The DAEs model is assumed to be index-1 and given in semi-explicit form. First, $K+1$ Gauss or Radau interpolation points are selected in finite element i. The differential, control, and algebraic profiles in a specified finite element i is approximated by Lagrange polynomial as follows:

$$\begin{aligned} &z^K(t)=\sum_{j=0}^{K}L_j(\tau)z_{ij}\\ &u^K(t)=\sum_{j=1}^{K}\bar{L}_j(\tau)u_{ij},\quad y^K(t)=\sum_{j=1}^{K}\bar{L}_j(\tau)y_{ij}\\ &L_j(\tau)=\prod_{k=0,\neq j}^{K}\frac{(\tau-\tau_k)}{(\tau_j-\tau_k)},\quad \bar{L}_j(\tau)=\prod_{k=1,\neq j}^{K}\frac{(\tau-\tau_k)}{(\tau_j-\tau_k)}\\ &\qquad t\in[t_{i-1},t_i], t=t_{i-1}+h_i\tau, \tau\in[0,1] \end{aligned} \tag{12}$$

where h_i refers to the length of the finite element i, and $0<\tau_j\leq 1, j=1,\ldots,K$ are the shifted Gauss or Radau points. This polynomial representation has the following property:

$$z^K(t_{ij})=z_{ij}, t_{ij}=t_{i-1}+\tau_j h_i \tag{13}$$

The continuity of the differential state profile at the finite element boundaries is enforced by the following expression:

$$\begin{aligned} &z_{i+1,0}=\sum_{j=0}^{K}L_j(1)z_{ij}, i=1,\ldots,N-1\\ &z_f=\sum_{j=0}^{K}L_j(1)z_{Nj}\\ &z_{1,0}=z_0 \end{aligned} \tag{14}$$

Substituting Eqs. (12)–(14) into Problem (11), collocation equation can be derived as follows:

$$\begin{aligned} &\sum_{j=0}^{K}\frac{dL_j(\tau_k)}{d\tau}z_{ij}-h_i f(z_{ik},y_{ik},u_{ik})=0\\ &z_{i+1,0}-\sum_{j=0}^{K}L_j(1)z_{ij}=0\\ &g(z_{ik},y_{ik},u_{ik})=0, i=1,\ldots,N, k=1,\ldots,K \end{aligned} \tag{15}$$

Eventually, the dynamic optimization problem is discretized into an NLP formulation with fixed finite element h_i, as follows:

$$\begin{aligned} &\min\ \Phi(z_f)\\ &s.t.\quad \sum_{j=0}^{K}\frac{dL_j(\tau_k)}{d\tau}z_{ij}-h_i f(z_{ik},y_{ik},u_{ik})=0\\ &\qquad g(z_{ik},y_{ik},u_{ik})=0\\ &\qquad u_L\leq u_{ik}\leq u_U, k=1,\ldots,K, i=1,\ldots,N\\ &\qquad z_{i+1,0}=\sum_{j=0}^{K}L_j(1)z_{ij}, i=1,\ldots,N-1\\ &\qquad z_f=\sum_{j=0}^{K}L_j(1)z_{Nj}, z_{1,0}=z_0\\ &\qquad \psi(z_f)\leq 0 \end{aligned} \tag{16}$$

The resulting NLP problem can be solved by a highly-efficient solver such as SNOPT [24] and IPOPT [25].

4. Adaptive mesh refinement strategy

For the fuel-optimal lunar descent problem with bounded magnitude of thrust, the optimal thrust profile typically has a "bang-bang" profile [23], thus breakpoints exist in the optimal thrust profile. In this section, the simplified lunar soft landing problem is defined. It is desired to transfer the system Eq. (1) from a specified initial state to a specified terminal state with admissible controls satisfying:

$$0 \le T \le T_{\max} \tag{17}$$

The performance measure to be minimized is expressed as follows:

$$J = -m(t_f) \tag{18}$$

where t_f is free. Using the state equation and the performance measure, the Hamiltonian profile is derived as follows:

$$\begin{aligned} H(t) &= \lambda_x V_x + \lambda_y V_y + \lambda_z V_z \\ &+ \lambda_{V_x}\left(\frac{T}{m}\cos\varphi\cos\phi - \frac{\mu x}{(x^2+y^2+z^2)^{3/2}}\right) \\ &+ \lambda_{V_y}\left(\frac{T}{m}\sin\varphi\cos\phi - \frac{\mu y}{(x^2+y^2+z^2)^{3/2}}\right) \\ &+ \lambda_{V_z}\left(-\frac{T}{m}\sin\phi - \frac{\mu z}{(x^2+y^2+z^2)^{3/2}}\right) + \lambda_m\left(-\frac{T}{I_{sp}g_0}\right) \end{aligned} \tag{19}$$

Then, the Hamiltonian profile can be simplified as follows:

$$H(t) = \lambda_x V_x + \lambda_y V_y + \lambda_z V_z - \left(\frac{\mu(\lambda_{V_x}x + \lambda_{V_y}y + \lambda_{V_z}z)}{(x^2+y^2+z^2)^{3/2}}\right) + TG$$

$$\text{where } G = \left(\frac{1}{m}(\lambda_{V_x}\cos\varphi\cos\phi + \lambda_{V_y}\sin\varphi\cos\phi - \lambda_{V_z}\sin\phi) - \frac{\lambda_m}{I_{sp}g_0}\right) \tag{20}$$

where λ_x, λ_y, λ_z, λ_{Vx}, λ_{Vy}, λ_{Vz}, and λ_m are costate variables.

The optimal control must satisfy the following expression:

$$\begin{aligned} &H(x^*, y^*, z^*, V_x^*, V_y^*, V_z^*, m^*, \varphi^*, \phi^*, T(t)^*) \\ &\le H(x^*, y^*, z^*, V_x^*, V_y^*, V_z^*, m^*, \varphi^*, \phi^*, T(t)) \end{aligned} \tag{21}$$

for all admissible $T(t)$, and for all $t \in [t_0, t_f]$; therefore,

$$T^*(t) = \begin{cases} 0, & \text{for } G > 0 \\ T_{\max}, & \text{for } G < 0 \\ \textit{Unknown}, & \text{for } G = 0 \end{cases} \tag{22}$$

The previously presented theoretical analysis reveals that the optimal thrust solution can easily have a "bang-bang" profile.

A novel adaptive mesh refinement strategy based on a constant Hamiltonian profile is proposed in this section to address the breakpoints in the optimal thrust profile. For Problem (11), Hamiltonian function is defined as follows:

$$\begin{aligned} H(t) &= \lambda(t)^T f(z(t), y(t), u(t)) + \eta(t)^T g(z(t), y(t), u(t)) \\ &+ \alpha^L(t)^T(u(t) - u_L) + \alpha^U(t)^T(u_U - u(t)) \end{aligned} \tag{23}$$

where λ, η, α^L, and α^U are the adjoint profiles. Therefore, the necessary condition of optimality for Problem (11) can be written as follows:

$$\begin{aligned} &\frac{d\lambda}{dt} = -\frac{\partial H}{\partial z}, \lambda(t_f) = \frac{\partial\Phi(t_f)}{\partial z} + \frac{\partial\psi(t_f)}{\partial z}\eta_f \\ &\frac{\partial H}{\partial y} = 0, \frac{\partial H}{\partial u} = 0 \\ &0 \le \eta_f \perp \psi(t_f) \le 0 \\ &0 \le \alpha_l^L(t) \perp (u(t) - u_L) \ge 0 \\ &0 \le \alpha_l^U(t) \perp (u_U - u(t)) \ge 0 \end{aligned} \tag{24}$$

where $x \perp y$ indicates that the elements have either $x = 0$ or $y = 0$, or both.

Problem (11) is an autonomous problem because it is not an explicit function of t. For an autonomous problem, the Hamiltonian is continuous and constant over time [26], such that:

$$\begin{aligned} \frac{dH}{dt} &= \frac{\partial H}{\partial z}\frac{dz}{dt} + \frac{\partial H}{\partial \lambda}\frac{d\lambda}{dt} + \frac{\partial H}{\partial y}\frac{dy}{dt} + \frac{\partial H}{\partial \eta}\frac{d\eta}{dt} \\ &+ \frac{\partial H}{\partial \alpha^L}\frac{d\alpha^L}{dt} + \frac{\partial H}{\partial \alpha^U}\frac{d\alpha^U}{dt} + \frac{\partial H}{\partial u}\frac{du}{dt} = 0 \\ H(t) &= \tilde{H} \end{aligned} \tag{25}$$

where $\tilde{H}$ is a constant. This condition is particularly useful for the detection of breakpoint locations. If the mesh does not capture the breakpoints, then the solution will not be optimal and the Hamiltonian profile near the breakpoints will not be constant, which illustrate that the mesh should be refined by adding new finite elements. As such, the finite element can be inserted into the position where the Hamiltonian is not constant. Furthermore, a stopping criterion can be established based on the constant Hamiltonian profile.

Ref. [27] showed that the Hamiltonian can be approximated at the collocation points as follows:

$$\begin{aligned} H_{ik} &= H_{(i-1)K+k} = \lambda_{ik}^T f(z_{ik}, y_{ik}, u_{ik}) + \eta_{ik}^T g(z_{ik}, y_{ik}, u_{ik}) \\ &= \frac{\bar{\lambda}_{ik}^T}{\omega_k h_i}\sum_{j=0}^{K}\frac{dL_j(\tau_k)}{d\tau}z_{ij} \\ \lambda_{ik} &= \bar{\lambda}_{ik}/\omega_k \end{aligned} \tag{26}$$

where $\bar{\lambda}_{ik}$ is the corresponding Karush-Kuhn-Tucker multiplier from Problem (16) and ω_k is the quadrature weight. When the Hamiltonian profile, represented by Eq. (26), is constant over time, the solution is sufficiently optimal.

The proposed adaptive mesh refinement strategy is given as follows:

Step 1: Divide the time domain equally with a small number of finite elements N, and solve Eq. (16) to provide an initial guess.

Step 2: First, calculate H_{ik} from Eq. (26), then find $(i*, k*)$ from

$$\begin{aligned} &(i^*, k^*) = \max_{ik}\left|H_{ik} - \tilde{H}\right| \\ &i = 1, \ldots, N, k = 1, \ldots, K \\ &\text{where } \tilde{H} = \left(\sum_{i=1}^{N}\sum_{k=1}^{K}H_{ik}\right)/(N \times K) \end{aligned} \tag{27}$$

We define the criterion in Eq. (27) to locate the index (i^*, k^*) where $H_{i^*k^*}$ deviates from the average value $\tilde{H}$ most. If $|H_{i^*k^*} - \tilde{H}| \ge \varepsilon$ (a specified small value), then proceed to Step 3; otherwise skip to Step 5.

Step 3: If $k^* \in [1, K-1]$, then divide the finite element i^* at the position of the k^*th collocation point, as follows:

$$\begin{aligned} N &= N + 1 \\ h_{i+1} &= h_i, i = (N-1)\ldots(i^*+1) \\ h_{i^*+1} &= h_{i^*} \times (1 - \tau_{k^*}), h_{i^*} = h_{i^*} \times \tau_{k^*} \\ \sum_{i=1}^{N} h_i &= t_f \end{aligned} \tag{28}$$

where τ_{k^*} is the k^*th Gauss or Radau point. Otherwise, divide the finite element i^* at the position of the $(K-1)$th

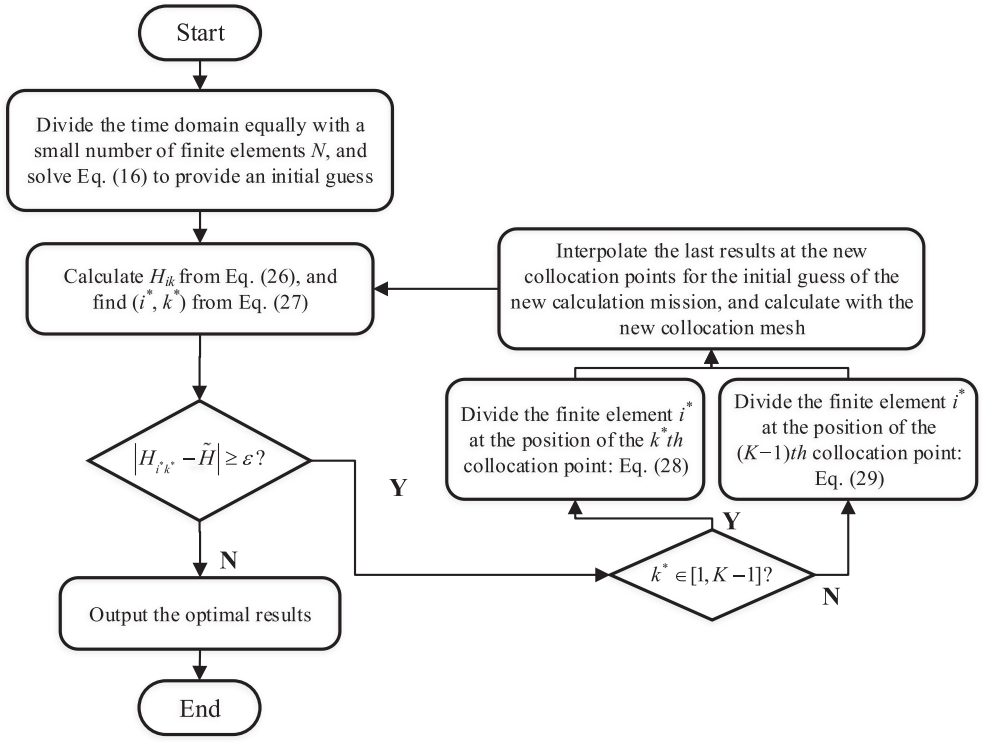

Fig. 2. Flowchart of the proposed adaptive mesh refinement strategy.

collocation point, as follows:

$$\begin{aligned} N &= N+1 \\ h_{i+1} &= h_i, i = (N-1)\ldots(i^*+1) \\ h_{i^*+1} &= h_{i^*} \times (1-\tau_{(K-1)}), h_{i^*} = h_{i^*} \times \tau_{(K-1)} \\ \sum_{i=1}^{N} h_i &= t_f \end{aligned} \tag{29}$$

where $\tau_{(K-1)}$ is the $(K-1)$th Gauss or Radau point. Then, proceed to Step 4.

Step 4: Interpolate the last results at the new collocation points for the initial guess of the new calculation mission to enhance the convergence of the solution. Calculate with the new collocation mesh. Subsequently, return to Step 2.

Step 5: Output the optimal results.

The flowchart of the proposed adaptive mesh refinement strategy is presented in Fig. 2.

5. Results and discussions

This section presents the results of simulations performed in AMPL environment [28], on a Lenovo Y430p running Windows 7 with an Intel® Core i7-4710MQ 2.50 GHz processor and 4 GB RAM. The version of the adopted NLP solver IPOPT is 3.8.0. The collocation points are three-order Radau points (i.e., $K=3$). The lunar soft landing data are mainly from Apollo12 [29]. The critical parameters are listed in Table 1. Two cases are simulated. The engine of the first case is throttleable between zero and full thrust. The Engine of the second case is throttleable between 10% and 60% of full thrust, and at full thrust. The number of finite elements for the general simultaneous dynamic optimization approach is 10 (i.e., $N=10$).

Table 1
Specifications for lunar soft landing.

Symbol	Value	Symbol	Value
H_0	R_M +15.7 km	V_{z0}	0 m/s
A_0	−1.43°	T_{max}	43,148.0 N
B_0	−8.43°	I_{sp}	302.39 s
γ	285.30°	m_0	15,234.0 kg
H_f	R_M	$\omega_{\alpha\ max}$, $\omega_{\beta\ max}$	5.0 °/s
A_f	−23.45°	μ	4.9028e12 m^3/s^2
B_f	−2.94°	R_M	1738 km
V_{x0}	1694 m/s	g_0	9.80 m/s^2
V_{y0}	−7.0 m/s	ε	1.0e−3

5.1. Case 1

5.1.1. Results obtained by the general simultaneous approach

The duration of the overall lunar descent process is approximately 632.0 s. Figs. 3a, b, and c show the position of the LM vs. time, which is transformed from the position vector (x, y, z). As shown in Fig. 3a, b, and c, the LM finally lands at the specified landing point (−23.45°, −2.94°, 0 m). Fig. 3d, e, and f show the velocity vector of the LM vs. time. Fig. 3d, e, and f show that the velocity vector eventually equals zero when the LM lands on the lunar surface. The tangential velocity gradually decreases to zero, and the radial and lateral velocities change with curves similar to parabolas.

Fig. 3g and h show the pitch and yaw angles of the LM vs. time. Fig. 3i and j reflect the angular rate of the pitch and yaw angles vs. time, satisfying the requirements of the specified range of the angular rate. The pitch and yaw angles change slightly in the lunar soft landing process, which is almost linear.

Fig. 3k and l show the thrust and mass profiles. The thrust of the LM is throttleable. Fuel consumption rate depends on the thrust magnitude. When the thrust is full, the mass of the LM sharply decreases. The magnitude of the thrust changes at the

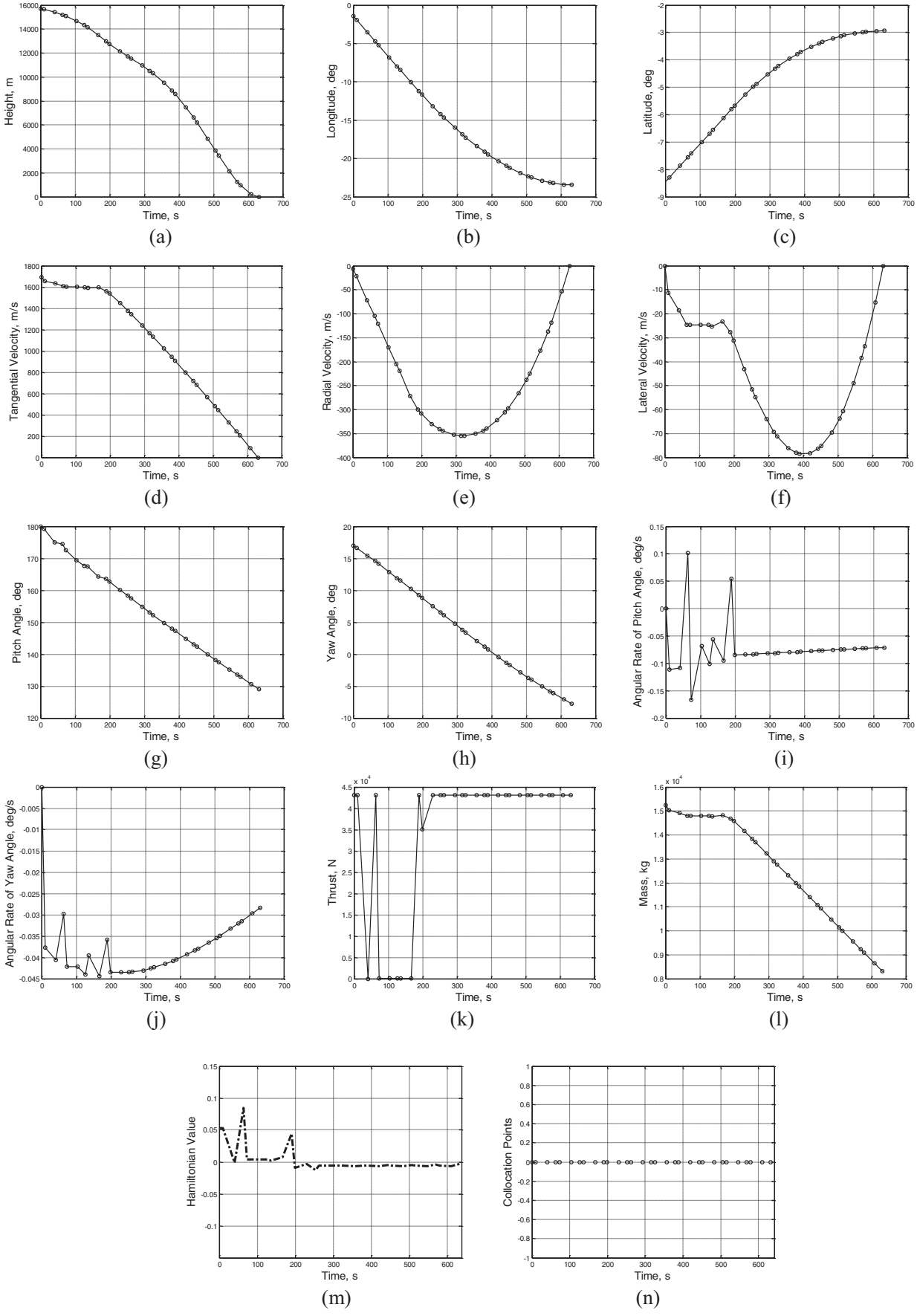

Fig. 3. Results obtained by the general simultaneous approach (Case 1).

maximum and zero. Though the magnitude of the thrust satisfies the specified requirement, the thrust profile with intensive jumps shown in Fig. 3k does not satisfy the engineering practice. Obviously, the collocation point mesh does not capture the breakpoints in the thrust profile.

Fig. 3m shows the Hamiltonian profile of the lunar soft landing trajectory optimization problem. It can be seen from Fig. 3m that the Hamiltonian is not flat, which illustrates that the obtained solution is not optimal. Fig. 3n shows the collocation point profile in the entire time domain. The collocation points are located at each finite element with the same number.

5.1.2. Results obtained by the enhanced simultaneous approach

The Subfigures in Fig. 4 show that state and control variables all satisfy the specified flight constraints. The results of the state variables are similar to that obtained using the general simultaneous approach without adaptive mesh refinement strategy.

Fig. 4k and l show the thrust and mass profiles. It can be seen from Fig. 4k that the optimal thrust control consists of full thrust during initiation of the mission, then a period of zero thrust (free-fall), followed by full thrust until touchdown. The optimal thrust profile has a "bang-bang" profile. When the thrust is full, the mass of the LM decreases linearly with the fastest rate. When the engine turns off from 32.8 s to 194.5 s, the mass of the LM remains unchanged. The overall lunar soft landing process is burn-coast-burn. The two switching times are 32.8 s and 194.5 s, respectively.

Fig. 4m shows that the Hamiltonian profile is almost constant over time, which illustrates that the results are optimal. More refined results for the state and control variables shown in Fig. 4 are derived via the enhanced simultaneous approach with adaptive mesh refinement strategy.

Fig. 4n shows the collocation point profile in the entire time domain. The dense parts of the collocation points locate at the breakpoints in the thrust profile. The enhanced simultaneous approach with the adaptive mesh refinement strategy captures the breakpoints in the optimal thrust profile. The final number of the finite elements is 38.

5.2. Case 2

The real lunar descent engine is throttleable between 10% and 60% of full thrust, and at full thrust [30,31], which is formulated as follows:

$$T = (10\% * T_{\max} \le T \le 60\% * T_{\max}) \text{ or } T_{\max} \tag{30}$$

Union property of *R*-function method [32,33] is utilized to express the thrust constraints in the lunar soft landing trajectory optimization problem for solving. Originally, the *R*-function method proposed by Rvachev is applied to obtain solutions of boundary-value problems in mathematical physics. The *R*-function method can transform Boolean operations of sets into algebraic operations of functions as follows:

$$\begin{aligned} &\text{Union}: f_1 \cup f_2 = f_1 + f_2 + \sqrt{f_1^2 + f_2^2} \\ &\text{Intersection}: f_1 \cap f_2 = f_1 + f_2 - \sqrt{f_1^2 + f_2^2} \end{aligned} \tag{31}$$

where f_1 and f_2 are functions. Here, we define

$$\begin{aligned} F_1 &= 10\% * T_{\max} \le T \le 60\% * T_{\max} \\ F_2 &= T_{\max} \end{aligned} \tag{32}$$

Then we express Eq. (32) as follows:

$$\begin{aligned} F_1 &= (T - 10\% * T_{\max}) * (60\% * T_{\max} - T) \\ F_2 &= (T - T_{\max}) * (T_{\max} - T) \\ T &= [(T - 10\% * T_{\max}) * (60\% * T_{\max} - T) \ge 0] \\ &\quad \cup [(T - T_{\max}) * (T_{\max} - T) \ge 0] \end{aligned} \tag{33}$$

Therefore, based on the union property of the *R*-function method, the thrust constraint Eq. (30) is written as follows:

$$F_1 \cup F_2 = F_1 + F_2 + \sqrt{F_1^2 + F_2^2} \tag{34}$$

Remark: if $F_1 + F_2 + \sqrt{F_1^2 + F_2^2}$ is equal or larger than zero, then $F_1 \ge 0$ or $F_2 \ge 0$, which satisfies the requirement of the thrust constraint.

Thus, the initial Boolean operation in the thrust constraint Eq. (30) is transcribed into an algebraic constraint which can be used as the path constraint in the lunar soft landing trajectory optimization problem. The obtained algebraic thrust constraint is expressed as follows:

$$\begin{aligned} &F_1 \cup F_2 = F_1 + F_2 + \sqrt{F_1^2 + F_2^2} \ge 0 \\ &\text{where } F_1 = (T - 10\% * T_{\max}) * (60\% * T_{\max} - T), \\ &\qquad F_2 = (T - T_{\max}) * (T_{\max} - T) \end{aligned} \tag{35}$$

In Case 2, the path constraint Eq. (2) is replaced by Eq. (35).

5.2.1. Results obtained by the general simultaneous approach

For Case 2, the duration of the overall lunar descent process is approximately 634.4 s. Fig. 5a, b, and c show that the LM finally lands at the specified landing point (−23.45°, −2.94°, 0 m). Fig. 5d, e, and f show that the velocity vector eventually equals zero when the LM lands on the lunar surface. As shown in Fig. 5i and j, the angular rate of the pitch and yaw angles satisfy the requirements of the specified range of the angular rate. The pitch and yaw angles almost change linearly in the lunar soft landing process, as shown in Fig. 5g and h.

As shown in Fig. 5k, the magnitude of the thrust changes at the maximum and minimum. Though the magnitude of the thrust satisfies the specified requirement, the thrust profile with intensive jumps shown in Fig. 5k does not satisfy the engineering practice. It can be seen from Fig. 5m that the Hamiltonian is not flat, which illustrates that the obtained solutions are not optimal. Obviously, the collocation point mesh does not capture the breakpoints in the thrust profile. The collocation point mesh needs to be refined.

5.2.2. Results obtained by the enhanced simultaneous approach

As shown in Fig. 6m, the Hamiltonian profile is almost constant over time, which illustrates that the results are optimal. Moreover, more refined results for state and control variables shown in Fig. 6 are derived via enhanced simultaneous approach with adaptive mesh refinement strategy.

Fig. 6k shows that the thrust profile satisfies the specified thrust constraints. The magnitude of the optimal thrust profile is between 10% and 60% of full thrust, and at full thrust. It can be seen from Fig. 6k that the optimal thrust control consists of full thrust during initiation of the mission, then a period of minimum thrust, followed by full thrust until touchdown. The optimal thrust profile also has a "bang-bang" profile. The two switching times are 24.3 s and 199.4 s, respectively.

As shown in Fig. 6n, the dense parts of the collocation points locate at the breakpoints in the thrust profile. The enhanced simultaneous approach with the adaptive mesh refinement strategy captures the breakpoints in the optimal thrust profile. The final number of the finite elements is 27.

6. Conclusion

In this study, an enhanced simultaneous dynamic optimization framework to determine the fuel-optimal trajectory of lunar soft landing with variable-thrust propulsion is presented. The thrust profile with piecewise property is formulated in the trajectory optimization problem by utilizing the Union property of *R*-function method. The optimal thrust profile in this study has a "bang-bang"

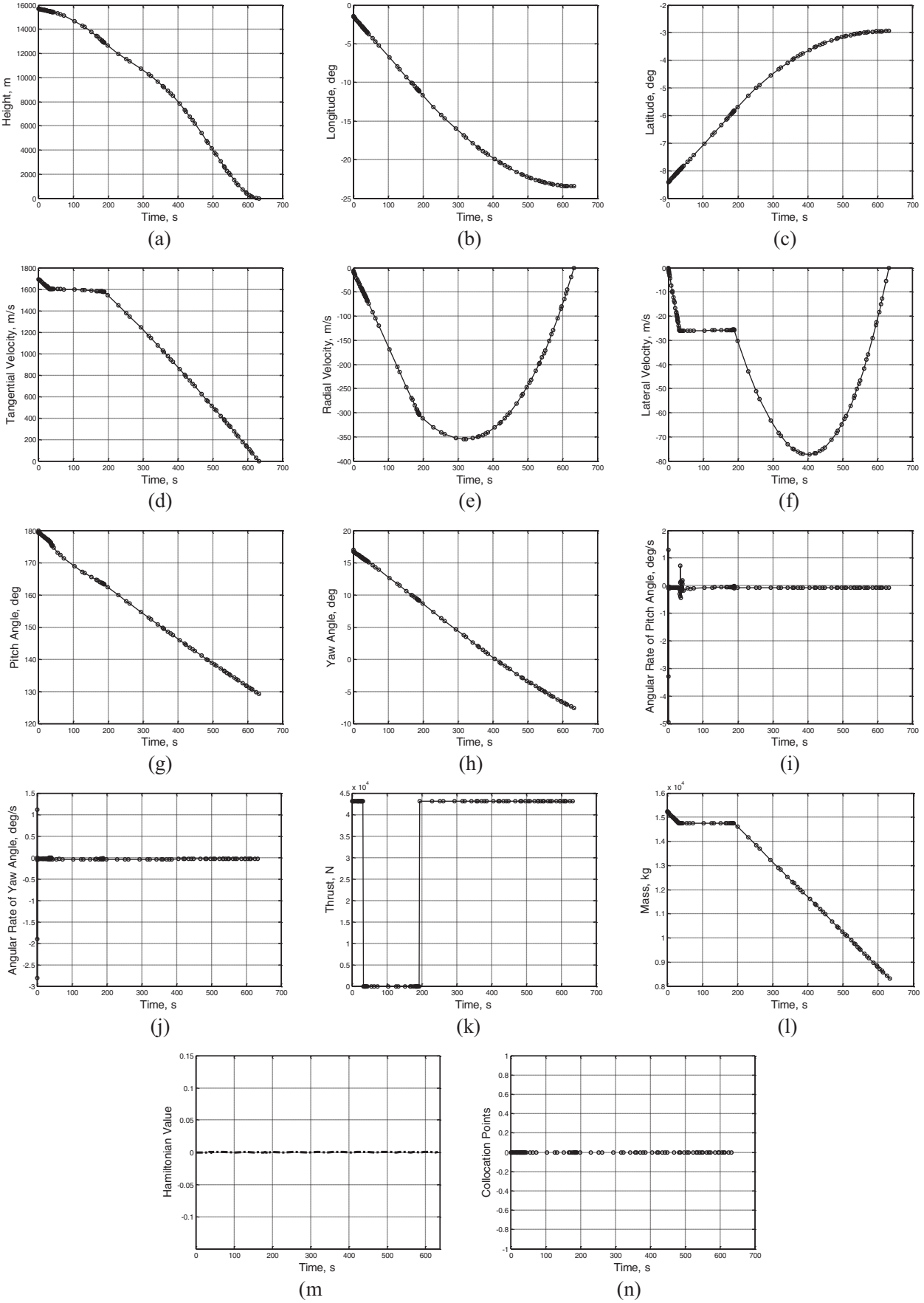

Fig. 4. Results obtained by the enhanced simultaneous approach (Case 1).

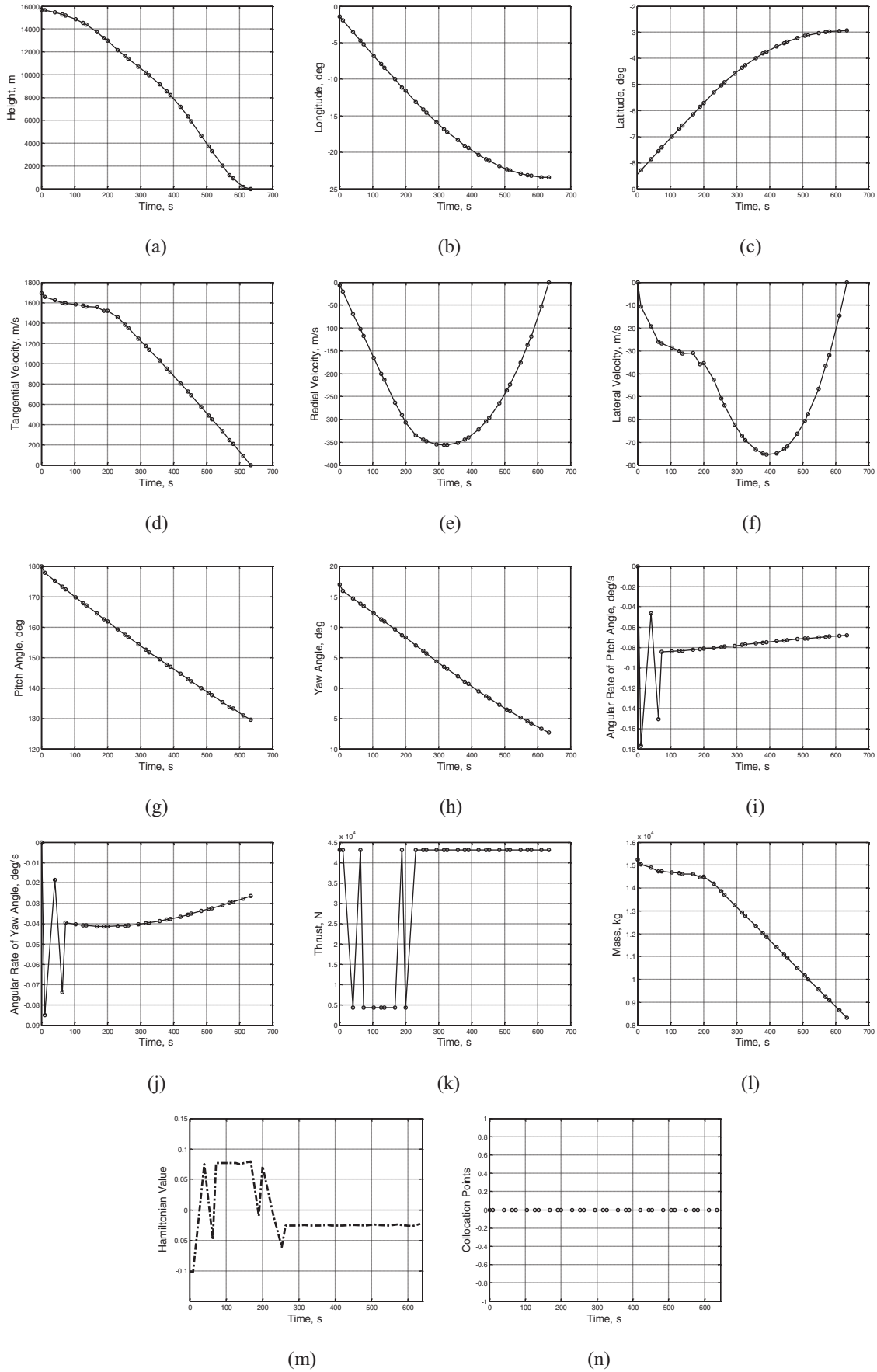

Fig. 5. Results obtained by the general simultaneous approach (Case 2).

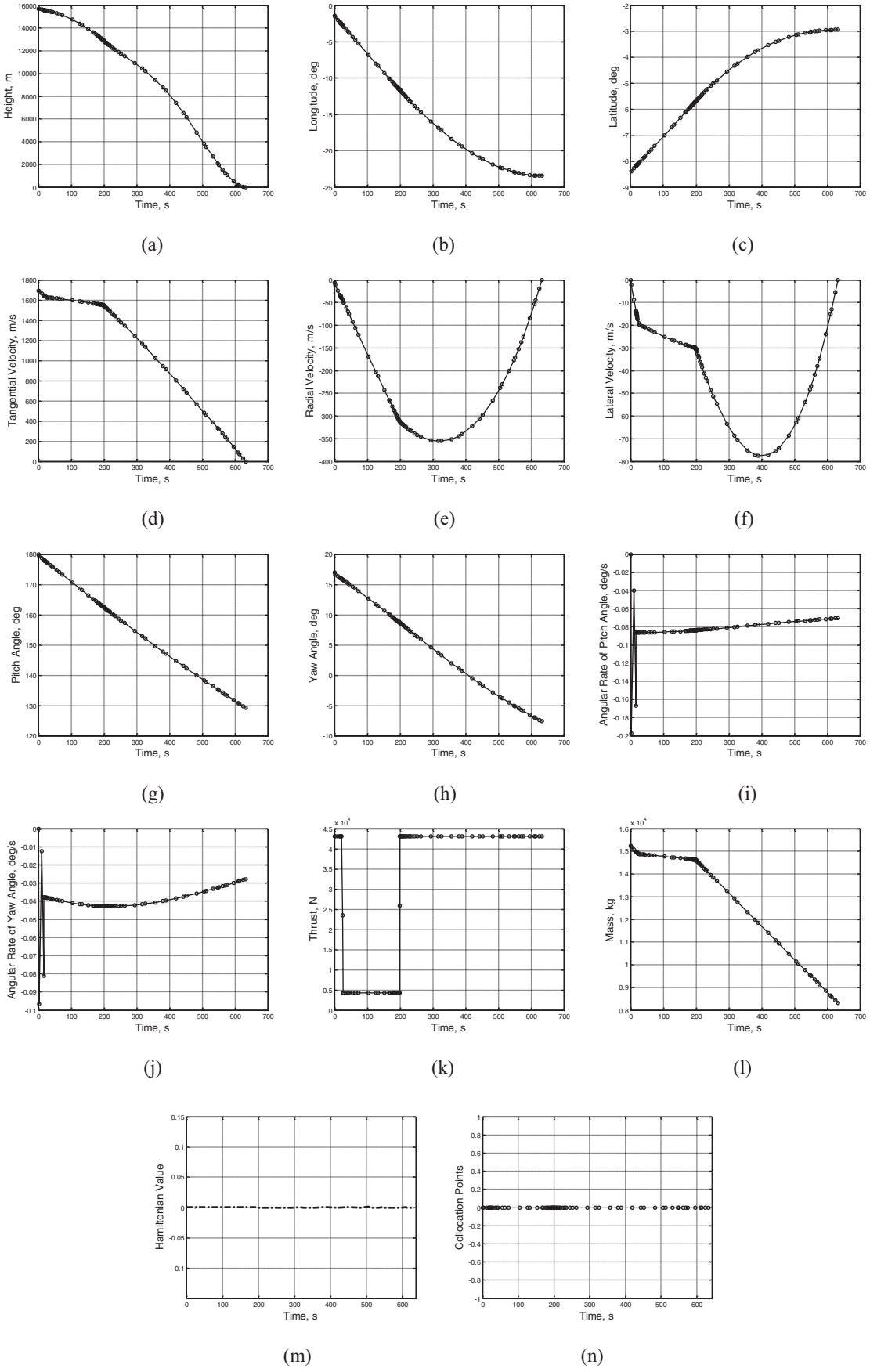

Fig. 6. Results obtained by the enhanced simultaneous approach (Case 2).

profile, which results in the existence of breakpoints in the optimal thrust profile. A novel adaptive mesh refinement strategy is proposed to capture the breakpoints in the thrust profile. The proposed mesh refinement strategy can add finite elements to the collocation point mesh based on a constant Hamiltonian profile, which is adaptive and efficient rather than add a large number of finite elements equally to the mesh. Compared with the general simultaneous dynamic optimization approach, the proposed enhanced simultaneous dynamic optimization approach with adaptive mesh refinement strategy can effectively capture the breakpoints of optimal thrust profile, and obtain more refined lunar soft landing optimal trajectory. The adaptive mesh refinement strategy is quite time-consuming. Thus, several additional heuristics could be considered to accelerate the adaptive mesh refinement strategy in the future.

A clear trend in the field of aerospace guidance and control, called “computational guidance and control” (CG&C), has recently emerged. The traits of CG&C are critical for system autonomy and support of autonomous operations. Optimized solutions based on model or data are desired or even necessary in CG&C. Consequently, the success of CG&C likely demands more up-front investment in formulating, modeling, and analyzing the problem. The enhanced simultaneous dynamic optimization framework for lunar soft landing is beneficial to the up-front investment of CG&C, which may eventually benefit the future autonomous lunar descent missions.

Acknowledgments

This research was supported by the 973 Program of China (No. 2012CB720503) and the National Nature Science Foundation of China (No. 61203132).

References

[1] Ahn JS, Park BG, Tahk MJ. Two-dimensional trajectory optimization of a soft lunar landing from a parking orbit considering a landing site. In: IFAC symposium on automatic control in aerospace, 18; 2010. p. 178–83. doi:10.3182/20100906-5-JP-2022.00031.
[2] Park BG, Tahk MJ. Three-dimensional trajectory optimization of soft lunar landings from the parking orbit with considerations of the landing site. Int J Control Autom Syst 2011;9(6):1164–72. doi:10.1007/s12555-011-0618-0.
[3] Boere M. Optimization of descent trajectories for lunar base settlement. Faculty of Aerospace Engineering Astrodynamics & Space Missions, Delft University of Technology; 2010. Master Dissertation.
[4] Young A. The twenty-first century commercial space imperative. New York: Springer; 2015. p. 43–57. doi:10.1007/978-3-319-18929-1.
[5] Meditch JS. On the problem of optimal thrust programming for a lunar soft landing. IEEE Trans Autom Control 1964;9(4):477–84. doi:10.1109/tac.1964.1105758.
[6] Cho DH, Jeong BY, Lee DH, Bang H. Optimal perilune altitude of lunar landing trajectory. Int J Aeronaut Space Sci 2009;10(1):67–74. doi:10.5139/ijass.2009.10.1.067.
[7] Pontani M, Cecchetti G, Teofilatto P. Variable-time-domain neighboring optimal guidance, Part 2: application to lunar descent and soft landing. J Optim Theory Appl 2015;166(1):93–114. doi:10.1007/s10957-014-0675-7.
[8] Zhou JY, Teo KL, Zhou D, Zhao GH. Nonlinear optimal feedback control for lunar module soft landing. J Global Optim 2011;52(2):211–27. doi:10.1007/s10898-011-9659-4.
[9] Chomel CT, Bishop RH. Analytical lunar descent guidance algorithm. J Guid Control Dyn 2009;32(3):915–26. doi:10.2514/1.37700.
[10] Liu XL, Duan GR, Teo KL. Optimal soft landing control for moon lander. Automatica 2008;44(4):1097–103. doi:10.1016/j.automatica.2007.08.021.
[11] Betts JT. Survey of numerical methods for trajectory optimization. J Guid Control Dyn 1998;21(2):193–207. doi:10.2514/2.4231.
[12] Benson DA, Huntington GT, Thorvaldsen TP, Rao AV. Direct trajectory optimization and costate estimation via an orthogonal collocation method. J Guid Control Dyn 2006;29(6):1435–40. doi:10.2514/1.20478.
[13] Chen W, Shao Z, Biegler LT. A bilevel nlp sensitivity-based decomposition for dynamic optimization with moving finite elements. AIChE J 2014;60(3):966–79. doi:10.1002/aic.14339.
[14] Elnagar G, Kazemi MA, Razzaghi M. The pseudospectral legendre method for discretizing optimal control problems. IEEE Trans Autom Control 1995;40(10):1793–6. doi:10.1109/9.467672.
[15] Fahroo F, Ross IM. Costate estimation by a legendre pseudospectral method. J Guid Control Dyn 2001;24(2):270–7. doi:10.2514/2.4709.
[16] Fahroo F, Ross IM. Pseudospectral methods for infinite-horizon nonlinear optimal control problems. J Guid Control Dyn 2008;31(4):927–36. doi:10.2514/1.33117.
[17] Garg D, et al. Direct trajectory optimization and costate estimation of finite-horizon and infinite-horizon optimal control problems using a radau pseudospectral method. Comput Optim Appl 2009;49(2):335–58. doi:10.1007/s10589-009-9291-0.
[18] Kameswaran S, Biegler LT. Convergence rates for direct transcription of optimal control problems using collocation at radau points. Comput Optim Appl 2008;41(1):81–126. doi:10.1007/s10589-007-9098-9.
[19] Vlassenbroeck J, Dooren RV. A chebyshev technique for solving nonlinear optimal control problems. IEEE Trans Autom Control 1988;33(4):333–40. doi:10.1109/9.192187.
[20] Garg D, et al. A unified framework for the numerical solution of optimal control problems using pseudospectral methods. Automatica 2010;46(11):1843–51. doi:10.1016/j.automatica.2010.06.048.
[21] Kameswaran S, Biegler LT. Simultaneous dynamic optimization strategies: recent advances and challenges. Comput Chem Eng 2006;30(10):1560–75. doi:10.1016/j.compchemeng.2006.05.034.
[22] Biegler LT. An overview of simultaneous strategies for dynamic optimization. Chem Eng Process 2007;46(11):1043–53. doi:10.1016/j.cep.2006.06.021.
[23] Lee AY. Fuel-efficient descent and landing guidance logic for a safe lunar touchdown. In: AIAA guidance, navigation, and control conference. AIAA; 2011. p. 2011–6499. doi:10.2514/6.2011-6499.
[24] Gill PE, Murray W, Saunders MA. SNOPT: an SQP algorithm for large-scale constrained optimization. SIAM J Optim 2002;12(4):979–1006. doi:10.1137/s1052623499350013.
[25] Wächter A, Biegler LT. On the implementation of an interior-point filter line-search algorithm for large-scale nonlinear programming. Math Prog 2006;106(1):25–57. doi:10.1007/s10107-004-0559-y.
[26] Stengel RF. Optimal control and estimation. New York: Dover Publications Inc.; 1994.
[27] Biegler LT, Campbell SL, Mehrmann V. Control and optimization with differential-algebraic constraints. Pennsylvania: SIAM; 2012. p. 241–59. doi:10.1137/9781611972252.
[28] Fourer R, Gay DM, Kernighan BW. A modeling language for mathematical programming. Manag Sci 1990;36(5):519–54. doi:10.1287/mnsc.36.5.519.
[29] Nolley JW. Apollo 12 (mission h-1) spacecraft dispersion analysis volume vi-dispersion summary; 1969. NASA TM–X–72099.
[30] Elverum GW, et al. The descent engine for the lunar module. In: Propulsion joint specialist conference; 1967. p. 67–521. doi:10.2514/6.1967-521.
[31] Dressler GA. Summary of deep throttling rocket engines with emphasis on apollo LMDE. In: AIAA/ASME/SAE/ASEE joint propulsion conference & exhibit. California: AIAA; 2006. p. 2006–5220. doi:10.2514/6.2006-5220.
[32] Rvachev VL, Sheiko TI. R-functions in boundary value problems in mechanics. Appl Mech Rev 1995;48(4):151–88. doi:10.1115/1.3005099.
[33] Kurpa L, Rvachev V, Ventsel E. The R-function method for the free vibration analysis of thin orthotropic plates of arbitrary shape. J Sound Vib 2003;261(1):109–22. doi:10.1016/s0022-460x(02)00946-x.